

Robust bidirectional continuous electrowetting based on metal–semiconductor (M–S) diodes

Qi Ni¹ · Daniel E. Capecci¹ · Millicent Schlafly¹ · Nathan B. Crane¹

Received: 25 May 2016 / Accepted: 5 August 2016 / Published online: 13 August 2016
© Springer-Verlag Berlin Heidelberg 2016

Abstract We demonstrate bidirectional continuous electrowetting by embedding metal–semiconductor diodes in the electrowetting substrate. Unlike conventional electrowetting on dielectric, bidirectional continuous electrowetting uses a single electrode pair to actuate a droplet through long distances. As long as the voltage potential is maintained between two end electrodes, the droplet moves toward the electrode with the higher potential. However, previously reported material systems had limited success in repeated actuation. In this work, diodes based on Schottky barriers were fabricated by forming metal–semiconductor junctions between titanium and high-resistivity n-type silicon. The performance enhancements were evaluated using current–voltage measurements of interface pairs. When the titanium is coated with gold to limit electrochemical reactions, the Schottky diodes achieved superior performance compared to electrochemical diodes previously studied. Droplet speed range from 8 to 240 mm/s is reported. Under repeated actuation, the speed of the droplet showed no degradation for up to 2000 cycles (experiment duration).

Keywords Droplet actuator · Reliable electrowetting · Electrochemical diodes · High-speed droplet actuation

1 Introduction

Electrowetting uses external electric field to manipulate discrete droplets on a planar surface (Mugele and Baret

2005; Nelson and Kim 2012). The most common configuration uses multiple electrodes on the substrate to create a voltage gradient under the droplet. The asymmetric voltage changes the apparent contact angles between the front and the back of the droplet to create an energy gradient that generates droplet motion. Compared to other droplet actuation methods such as magnetic (Nguyen et al. 2006) and surface acoustic (Wixforth et al. 2004), electrowetting generates larger actuation forces and is simpler to implement (Ni et al. 2015). The large force capability of electrowetting-driven actuation enables a wide range of droplet volumes to be manipulated; nanoliter to microliter droplet manipulation is common in electrowetting-based devices (Pollack et al. 2000). The substrate used can be readily fabricated by conventional semiconductor processes, and no external fixtures (channels/supports) are required.

Electrowetting, especially electrowetting on dielectric (EWOD), has been demonstrated in numerous lab-on-a-chip technology to perform operations such as pumping, mixing, splitting and merging droplets (Cho et al. 2003; Pollack et al. 2000). EWOD also finds application in optical fields such as variable focus lens (Berge 2005) and reflective display technology (Hayes and Feenstra 2003). Electrowetting can also be used to move droplets to perform mechanical tasks as an alternative to silicon-based microelectromechanical systems (MEMS)—out-of-plane motion was demonstrated in Knospe and Haj-Hariri (2012). Other in-plane actuation demonstrations include rotational/linear fluidic motors (Lee and Kim 2000; Takei et al. 2010), droplet-based conveyor system (Moon and Kim 2006) and fluidic switch (Sen and Kim 2009).

For mechanical actuation, common EWOD is analogous to electromagnetic motors in both actuation and control scheme. EWOD uses stepper-type actuation—the electrodes underneath the droplet are turned on and off

✉ Nathan B. Crane
ncrane@usf.edu

¹ Department of Mechanical Engineering, University of South Florida, 4202 E. Fowler Avenue, Tampa, FL 33620, USA

sequentially so the droplet can move to the next step. Continuous motion is accomplished by sequentially energizing each electrode. Similar to electromagnetic stepper motors, EWOD droplet actuation does not require position feedback as long as the actuation speed/force is within the system capability. If the electrode switching frequency or force is too high, the droplet will miss a step, the motion will stop, and the droplet position will be unknown. Electrical feedback such as impedance metering can be implemented to overcome the problem (Gong and Kim 2008); but additional hardware and control algorithm are required. In addition, the electrodes in EWOD are generally turned either fully on or fully off, which requires the droplet to take a full step each time though a method for open-loop microstepping was recently demonstrated (Ni et al. 2016). This in turn poses limitation on the maximum speed of the droplet can achieve. This can also introduce additional complications in design and wiring of the system. For example, if the droplet needs to travel a distance of 20 times the droplet diameter, twenty electrodes are needed. Through-hole and multilayer substrates are usually required to accommodate the number of interconnects and switches needed.

On the other hand, “Continuous Electrowetting Effect” modulates the electrical double layer between liquid metal (mercury) and electrolyte ambient solution (Lee and Kim 2000). Continuous motion is achieved by applying a voltage along the length of an enclosed microfluidic channel. The metal droplet will be propelled toward the lower potential electrode as long as the voltage is maintained. For linear actuation, only one pair of electrodes is needed. However, the speed of the droplet is limited by the maximum sustainable voltage of the electrical double layer (typically <math><1\text{ V}</math>). Closed channels and the use of hazardous mercury limit the applicable area of continuous electrowetting actuation.

Previously, we reported a different method to achieve continuous electrowetting based on the electrochemical effect of metal/electrolyte combination (Crane et al. 2010; Khodayari et al. 2014; Nelson et al. 2011). Electrolytic solutions were used to form/dissolve a thin protective oxide on valve metals such as aluminum and titanium. The electrolyte/electrode interface is effectively a diode which conducts current in one direction only. While these devices have shown reliable contact angle change (Khodayari et al. 2012b) and stable performance in pairs (Khodayari et al. 2014), these improvements did not translate to reliable actuation in the continuous electrowetting prototype devices. All of them have shown poor reliability when tested under repeated actuation. In search of better material combinations, a new type of diode is introduced. This paper reports the results of using embedded Schottky diodes on a high-resistivity silicon substrate to actuate electrolytic droplets. The current voltage behavior of electrochemical diodes and metal semiconductor diodes is compared by IV

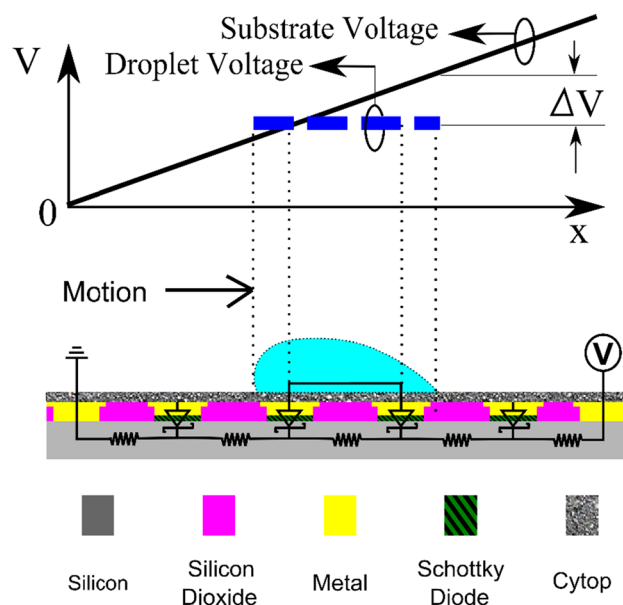


Fig. 1 Bidirectional continuous electrowetting principle. A voltage is applied between the ends (ohmic contacts) of a high-resistivity silicon substrate. A conductive droplet with negligible resistance bridges two diode sites. The diode in the front of the droplet is reverse biased while the diode in the back of the droplet is forward biased. The droplet’s potential is close to the potential of the substrate at the diode with lower voltage creating a voltage difference between the droplet and the substrate at the leading and trailing edges (ΔV). Since the voltage difference is larger on the high potential side, there is an asymmetrical electrowetting force that moves the droplet toward the higher potential electrode

measurements. Working prototypes are demonstrated, and the droplet’s speed and reliability data are reported.

2 Operating principle

The operating principle of the proposed device is illustrated in Fig. 1. An electric potential is applied across the length of the substrate (silicon wafer) to create a continuous voltage gradient. A high-resistivity wafer minimizes the required current and heating of the substrate under the applied voltage. When the conducting droplet bridges two or more diode sites, the diode in the high potential side (right) is reverse biased and no current is flowing. At the same time, the diode at the lower potential side (left) is forward biased due to the charge accumulation in the droplet. The effective potential difference induced by the substrate applies a force to the contact line in the front of the droplet and lowers the apparent contact angle. This in turn moves the droplet toward the higher voltage electrode. The same cycle repeats when the droplet moves to the next diode sites. The diode in the front of the droplet is always reverse biased, and the diode in the back side of the droplet is

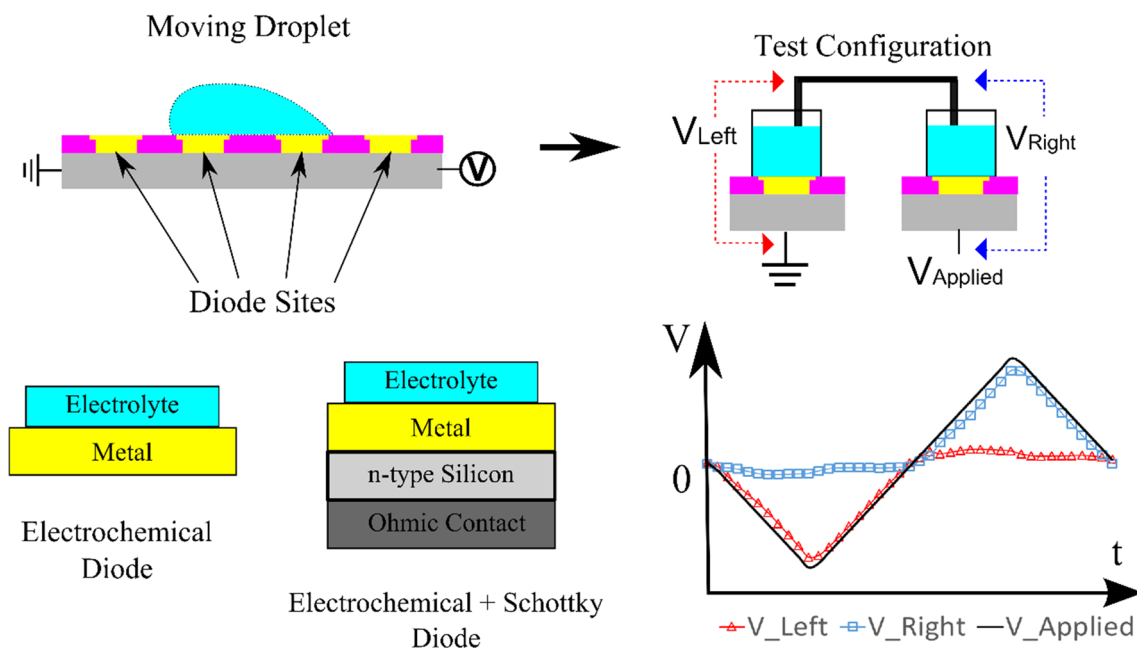


Fig. 2 Illustration of the tube measurements setup. *Top row*: the droplet under electrowetting actuation was split into two halves. The voltage of the electrolyte/substrate pair was then measured as a function of a bipolar input signal. *Bottom left*: electrochemical diode

alone. *Bottom middle*: Schottky and electrochemical diodes in series. *Bottom right*: an example of the voltages (V_{left} , V_{right}) response under excitation voltage ($V_{Applied}$) for electrochemical Schottky diodes

always forward biased. As long as the voltage is maintained between the ends of the substrate, the motion of the droplet is sustained. When the polarity of the voltage is switched, the droplet’s motion will follow the higher potential electrode (Nelson et al. 2011).

3 Electrochemical diodes combined with Schottky diodes

In our previous bidirectional continuous electrowetting demonstrations, the working diodes were based on electrochemical reactions during actuation. While electrochemical diode performance depends on both the electrolyte and the metal interface, Schottky diodes are based on solid-state semiconductor physics which potentially could be used with any conducting fluid. Schottky diodes are based on the potential barrier formed at metal–semiconductor junction. At thermal equilibrium, the metal–semiconductor interface has a built-in potential to ensure the fermi level is consistent within the junction (Arscott 2014). The resulting constant fermi level bends the energy band of the semiconductor. For lightly doped n-type silicon, most metals form Schottky barrier contacts. When a positive bias is applied to the metal, the fermi level of the metal is lowered and electrons flow. When the metal is negatively biased, the fermi energy of the metal increases and the potential barrier blocks current. The rectifying behavior of Schottky diodes

has been widely used in the electronic industry due to their fast switching time and low forward voltage drop (Olikh 2015). In electrowetting, Schottky junction formed by the electrolyte and silicon surface has been utilized to move droplets by light (photoelectrowetting) (Arscott 2011). Due to the different diode working mechanisms, the two diodes (electrochemical and Schottky) could be used simultaneously by connecting them in series—the electrochemical diodes work at the metal/electrolyte interface and the Schottky diodes work at the metal/silicon surface.

In continuous electrowetting devices, diode characterization is difficult because the droplet is continuously moving from one diode to another. Prior work has relied on a modified test arrangement using a single pair of diodes (Khodayari et al. 2014). For simplicity of measurement, the droplet is simulated by two electrically connected droplets (see Fig. 2, top). Each droplet sits on an identical diode. A triangular voltage input (ramping pattern: 0 to -50 to $+50$ to 0 volts at 0.5 volts/20 ms) is applied between the two substrates, and the voltages of the droplet and current through the droplet are measured using a two-channel source meter (Keithley 2612A).

The voltage cycle was repeated 2000 times with 5 s off time between the cycles. The voltage at the right side of the droplet was then calculated taking the difference between the applied voltage and droplet voltage.

The relative performance of the diodes in an actuator can be assessed by calculating the ratio of the resulting

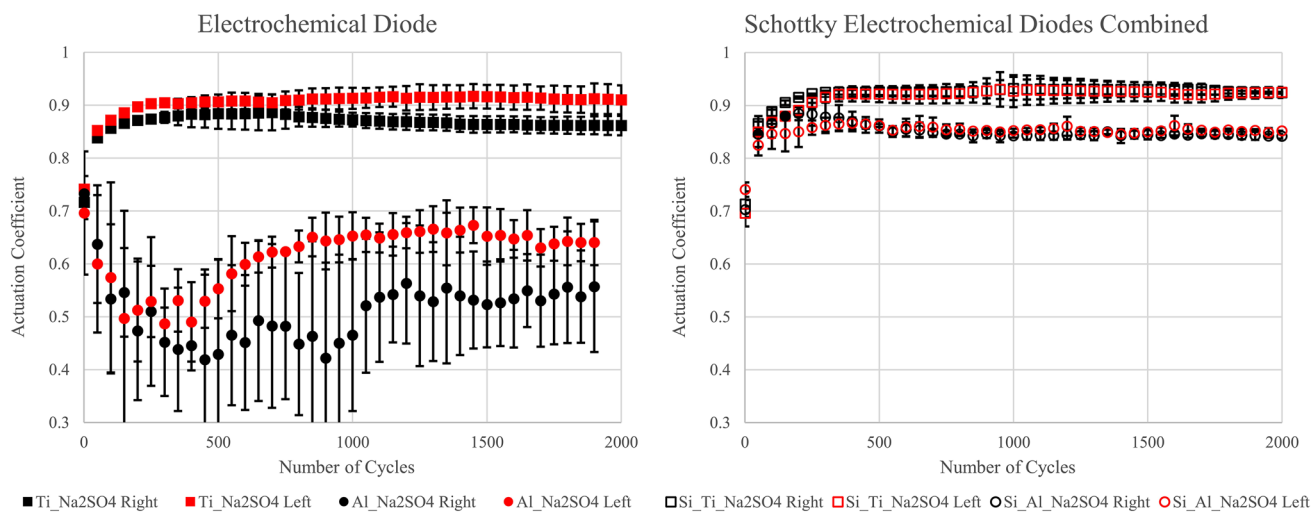


Fig. 3 Resulting actuation coefficient versus the number of actuation cycles with 0.1 M concentration Na_2SO_4 . The average values and standard deviation of three trials are plotted. *Left*: the electrochemical diode alone. *Right*: Schottky combined with electrochemical diodes

actuation force for the diode circuit over the actuation force of a grounded droplet with the same applied potential. The actuation force for a droplet over a substrate with a linearly varying voltage is found by integrating the electrowetting force around the circumference of the droplet. The net actuation force is

$$F = \frac{\epsilon_0 \epsilon_r}{4d} * (\pi * r) * \Delta V * (\Delta V - 2V_{\text{drop}}) \quad (1)$$

where $\epsilon_0 \epsilon_r$ is the dielectric permittivity, d is the thickness of the dielectric layer and r is the droplet radius. The voltages ΔV are the voltage difference between the leading and trailing edges of the droplet, and V_{drop} is the voltage of the droplet measured relative to the trailing edge. For the ideal case (grounded droplet), V_{drop} is zero. The actuation coefficient ($\eta_{\text{actuation}}$) is taken as the ratio of the actual force over the grounded droplet force is given by ($\eta_{\text{actuation}} = 1 - 2 \frac{V_{\text{drop}}}{V_{\text{applied}}}$) (see detailed derivation in Khodayari et al. 2014).

V_{drop} is always measured relative to the lower potential so if the applied potential is positive, V_{drop} would be the voltage on the left tube and if the applied voltage is negative, V_{drop} would be the voltage on the right tube. The coefficient was calculated using the left and right voltages to determine the actuation force of the diode system relative to a grounded droplet. An actuation coefficient of one represents the same actuation force as a grounded droplet system and is only possible with two ideal diodes (no voltage drop across the forward-biased diode, no current through the reverse-biased diode). When the actuation coefficient is zero, there is no polarity dependence in the “diodes” and no actuation force is produced. The resulting data in terms of actuation coefficient at peak voltage are plotted against

the number of testing cycles in Fig. 3. Each condition was repeated three times, and the average values are plotted. The error bars represent the standard deviation of each set.

We have previously reported diodes based on electrochemical reactions alone using metals and different electrolytes (Khodayari et al. 2014; Nelson et al. 2011). The best tested combination was titanium (Ti) with sodium sulfate (Na_2SO_4) electrolyte. Titanium and aluminum electrodes are included as a reference standard for the Schottky/electrochemical combined diodes.

The Schottky/electrochemical diode substrates (Fig. 2, bottom row) were fabricated using similar method described in the materials section below except that the ohmic contact was made at the backside of the wafer rather than the ends. I–V measurement with contacting probes confirmed the current rectifying behavior of the Schottky diodes. For electrochemical diode substrates (Fig. 2, bottom row), metal film (titanium or aluminum at 400 nm thickness) was evaporated onto clean glass slides (3×2 in, Corning®). Circular plastic tube (internal diameter: 8 mm, length: 10 mm) was attached to the front side of the diodes using epoxy. Before each test, the tubes were filled with electrolytes (0.1M Na_2SO_4) and the electrical connections to the tubes were made by inserting a 1-mm-diameter activated titanium electrode. All other connections were made using copper wires.

The data suggest the combination of Schottky and electrochemical diodes improved the performance of the electrowetting actuation in several ways. The first is that with the Schottky diodes, the left and right voltages are equal, whereas when electrochemical diodes were used alone, the resulting actuation coefficient was non-symmetrical (Fig. 3, left). The higher actuation coefficient on the left side indicated a better diode-like behavior for the left

metal/electrolyte interface. Since all experiments used a triangular wave which started from zero and ramped to negative peak (-50 volts) then positive (50 volts) then zero, the diode on the left would be reverse biased and the diode on the right would be in forward biased during the first half of each voltage cycle. This could cause the anodic oxide formation on the metal surfaces being non-symmetric with the oxide being thicker on the left; which would explain the behavior. When electrochemical diode is combined with Schottky diode, the additional Schottky diode prevented current flow in the initial cycle. As a result, the left and right actuation coefficients remained same (as shown in the plot on the right side of Fig. 3).

Additionally, the actuation coefficient was improved significantly with the inclusion of Schottky diodes. The aluminum showed particularly dramatic improvement, and the titanium reached a value of 0.92. The combination of aluminum and sodium sulfate is unsuitable due to the poor actuation coefficient as previously reported (Khodayari et al. 2014) and reconfirmed here (Fig. 3, left). But with the addition of Schottky diodes, the aluminum/sodium sulfate combination achieved a 0.85 actuation coefficient (Fig. 3, right) after 2000 actuation cycles compared to 0.65 with the electrochemical diode alone.

However, both diode types showed a lower actuation coefficient during the initial 100 cycles before reaching steady state. The average of the peak current magnitudes during the positive and negative sweep decreased significantly over the first 100 cycles as shown in Fig. 4. It is clear that incorporating the Schottky diodes drastically reduced the leakage current over electrochemical diodes alone. However, the initial higher currents in the combined diodes still introduce undesirable variation in actuation with time. Because the Schottky diodes still contain an electrochemical passivating interface (Ti/electrolyte or Al/electrolyte), the electrochemical diodes at the metal–electrolyte interface still experience some electrochemical reactions which caused the observed behavior.

While these tests show clear benefit from incorporating Schottky diodes, the diode current still changes with repeated cycling, likely due to the electrochemical interactions. This could still hinder the actuation in the initial cycles. To assess this effect, continuous EW actuators were fabricated using both combined electrochemical/Schottky diodes (titanium deposited on silicon and exposed directly to the electrolyte) and Schottky only diodes (500-nm gold overlayer shields the titanium from the electrolyte). The continuous EW performance of the two diode types was compared.

4 Materials and fabrication

All substrates were n-type (phosphorus) high-resistivity silicon wafers (100 mm diameter, 525 μm thick,

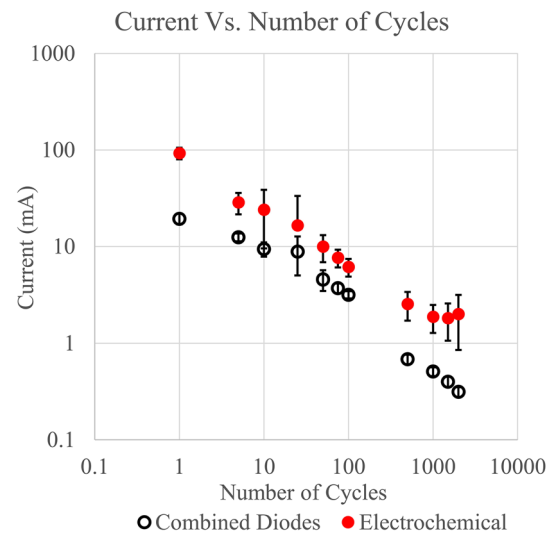


Fig. 4 Peak current magnitude during cyclic tube tests for electrochemical alone and electrochemical plus Schottky diodes. The average value of three tests is presented, and the *error bars* show the standard deviation of the data

orientation: 1–0–0, resistivity: 560–840 Ω cm). An oxide mask (~ 5000 Å thick) was grown using wet oxidation and then patterned to expose the silicon for end contacts (the extreme left and right points in Fig. 1). After standard RCA cleaning, phosphorus solid source diffusion was performed in a Bruce diffusion furnace to establish ohmic contacts for the end electrodes (nitrogen atmosphere, 40 min at 1000 $^{\circ}\text{C}$). The diode sites were protected using the oxide mask during diffusion. After diffusion, the oxide mask was removed using 49 % concentration hydrofluoric acid (HF). After another round of RCA cleaning, the wafers were processed in the furnace again to drive in the dopant (oxygen and hydrogen atmosphere, 60 min at 1050 $^{\circ}\text{C}$). The resulting oxide film from the drive-in process was then thinned down (buffered oxide etch (BOE), 6:1) to a final thickness of 2800 Å (± 200 Å) to serve as the dielectric in electrowetting actuation. It was suggested in Jaeger (2002) that thermal cycling could drive the dopant in the bulk to the surface of the silicon to alter the dopant concentration profile near the surface. This could interfere with reliable Schottky diode formation so the silicon at those locations was etched to a depth of ~ 1 μm using reactive ion etching (RIE). Titanium (1.5 μm) or titanium/gold (~ 0.75 μm each) was then evaporated onto the substrate and patterned by a lift-off process. The resulting diode sites had a silicon contact diameter of 250 μm . The metal spots (300 μm diameter) were designed to be slightly larger than the diode sites to assure full coverage of the exposed silicon.

To prevent the droplet under test from sliding off the substrate, 100- μm high SU-8 rails were patterned along the length of the wafer, as well as the ends before the ohmic

contacts. A ~ 30 -nm fluoropolymer Cytop[®] was applied as the top coat to enhance the non-wetting behavior of the droplet before the substrate was diced into individual actuators (32×7 mm). The fluoropolymer coating has negligible contribution to the dielectric due to its much smaller thickness. For all substrates, the actuation area was defined by the SU-8 rails (24×3 mm). For droplet speed testing, the diode center to center spacing was 2 mm. The spacing was chosen so the droplet ($60 \mu\text{L}$, diameter ~ 5 mm) could bridge at least two diode sites at any time (see Fig. 5, top).

5 Electrical measurements

The fabricated Schottky diodes were tested without electrochemical effects by connecting the grounding probe of a HP 4145B semiconductor analyzer to one end of the ohmic contact pad and sourcing probe to one of the diode sites. A voltage ramp was applied at the rate of $0.1 \text{ Volt}/0.1 \text{ s}$ while the voltage and current were recorded at the same rate. The peak-to-peak voltage ramp was set at -50 to 50 volts. Light and dark ambient conditions, titanium and titanium/gold metal layers as well as positive and negative ramps were tested with no observable difference due to light, ramp direction or gold overlayer. The IV curves are presented in Fig. 6. The dot number indicates the locations of the diode sites with one being closest to the grounding ohmic contact and 12 being the furthest away from the grounding probe. As expected, all diode sites conducted current when forwardly biased. Their decreasing slopes in the IV curves show the effect of increasing series resistance from the high resistance substrate as the spacing between the diode and the end contact increases. The end-to-end contacts showed linear behavior confirming ohmic contacts at both ends. The measured end-to-end resistance value was $70.8 \text{ k}\Omega$. Taking account of the test sample dimension (width: 7 mm , thickness: $525 \mu\text{m}$, length: 32 mm), the approximated resistivity was $813 \Omega \text{ cm}$, consistent with the wafer specification.

6 Droplet speed testing

The droplet was actuated under constant applied voltage to measure the actuation speed. All tests were performed in an oil ambient (silicon oil OS-30 from Dow Chemical Company) to reduce the effect of contact angle hysteresis. Each test used a fresh $60 \mu\text{L}$ (~ 5 -mm-diameter droplet) sodium sulfate aqueous solution with 0.1 M concentration. The test strip's end ohmic contacts were connected to a Masuzada[®] high voltage amplifier. An overhead camera was used to record the position of the droplet while a custom Labview[®] program acquired images at the rate of 50 Hz . The captured images were processed in MATLAB[®] image analysis tool

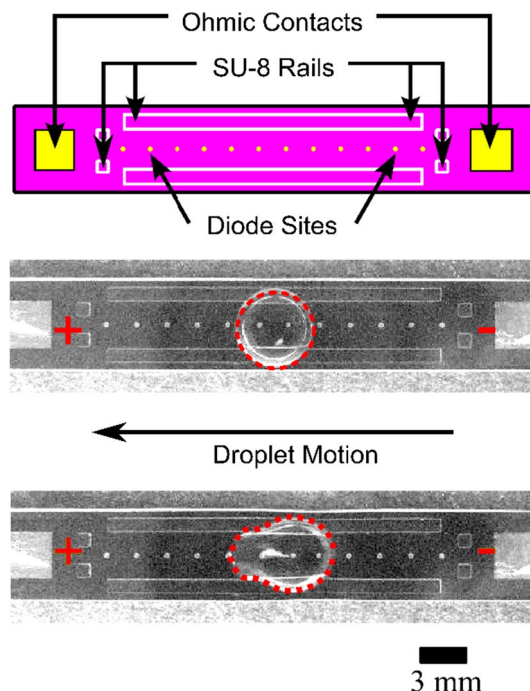


Fig. 5 Illustration of bidirectional actuation prototype. *Top*: test prototype design. *Middle*: droplet actuation under 150 V between the ohmic contacts, and the volume of the droplet was $60 \mu\text{L}$ (~ 5 -mm-diameter drop). *Bottom*: droplet actuation under 210 V between ohmic contacts. The *positive* and *negative signs* indicate the polarity of applied voltages, and the *dotted line* shows the outline of the droplets

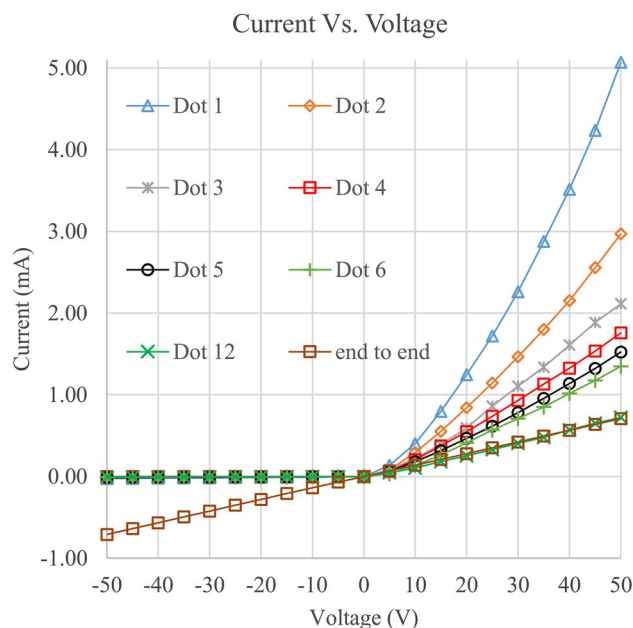


Fig. 6 Current–voltage measurements of the fabricated Schottky diodes. The *x*-axis is the measured voltage (V), and the *y*-axis is the measured current (mA). The *dot number* indicates the location of the diode sites with one being closest to the ohmic contact and 12 being the furthest away. The end-to-end contacts were also measured to extract the total resistance of the substrate

to extract the centroid of the droplet's position at each time point.

In complete device testing, only limited motion of the droplet was achieved by the electrochemical/Schottky combined diodes. The droplet would move in an unsteady stop/start motion or halt entirely part way. This is likely due to the initial low actuation coefficient in the combined diodes. However, the Cytop coating may also be contributing to reduced performance despite the porous nature of the thin film (30 nm). It would act as a self-healing dielectric on reverse-biased diodes (Dhindsa et al. 2011; Khodayari et al. 2012a, b). Additionally, the Cytop coating would decrease the electrical current through the diode due to reduced contact area between fluid and metal and slower transport through the film. This would grow worse with oxide growth after the initial excitation.

In contrast, actuators with Schottky diodes alone (titanium electrodes with gold coating) achieved repeatable actuation from the first. Therefore, further experiments were carried out using only the standalone Schottky diodes. The gold diodes would be less sensitive to the Cytop coating than titanium since the gold does not form a passivating oxide layer that reduces current flow. However, the Cytop may still reduce the current flow on the forward-biased diodes so that at high speeds, the assumption that the droplet is at the potential of the trailing diode may breakdown.

Average droplet velocities were measured by measuring the number of frames to traverse the strip. The resulting data are plotted against the actuation voltage in Fig. 7. The extracted average velocities range from 8 mm/s (150 V) to 240 mm/s (240 V). A parabolic fit is used to show the relation between the average velocities and the actuation voltages. Since the actuation force is related to the applied voltage squared (Young–Lippmann equation), it seems reasonable that the average velocities scale the same, as shown by other researchers (Bavière et al. 2007; Ren et al. 2002).

However, the frame-by-frame position versus time plot of the droplet actuation presented in Fig. 8 shows a more complex relationship. The applied voltages between the end contacts range from 150 V (minimum actuation voltage, Fig. 5 middle) to 240 V (limited by amplifier current capacity), which translates to a voltage gradient of 4.7–7.5 V/mm, respectively. Above 200 V, the large actuation force and/or drag forces from the oil ambient deformed the droplet and the image analysis methods could not accurately resolve the boundary of the droplet to extract reliable position data (Fig. 5, bottom).

For lower voltages (<170 V), the droplet accelerated and then decelerated to a lower steady state velocity, as shown in Fig. 8. Higher voltages (>180 V) did not show this deceleration over the length of the test strips, but it may have been seen if tested a longer test strip. The decrease in velocity after the initial ramp could be caused by increased losses due to contact line friction and the viscous shear within the

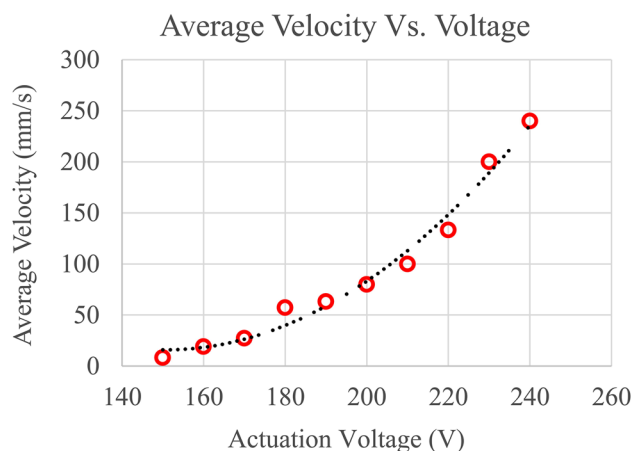


Fig. 7 Average velocity of the droplet versus the actuation voltage. The actuation voltages range from 150 to 240 V between the contacting electrodes (32 mm separation), and the volume of the droplet was kept constant at 60 μ L (~5-mm-diameter droplet)

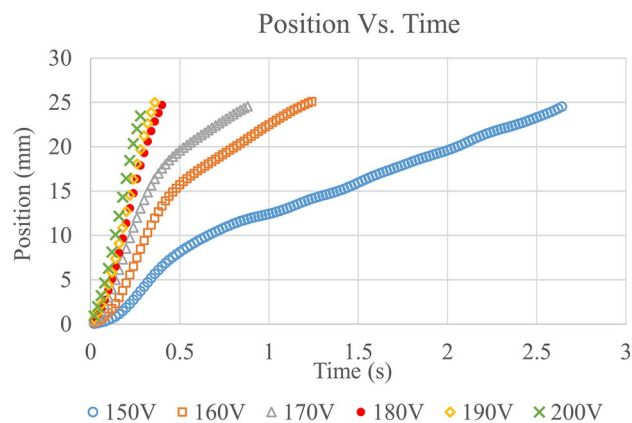


Fig. 8 Droplet centroid's position versus time for different applied voltages

droplet or due to the droplet moving through the oil ambient. Due to localized electrowetting force, the resulting contact line friction and viscous shear stress could be significant (Bavière et al. 2007), especially for large droplet, as suggested in (Ren et al. 2002). The droplet was assumed to be under constant actuation force due to the fixed width of the substrate (the force per unit contact line is fixed), but at higher speeds and with more than two diodes in contact at one time, this assumption may not be accurate. Additional work is needed to identify the reason for the deceleration.

7 Actuation reliability

For the above droplet speed tests, the spacing between the diodes was chosen to ensure the droplet could bridge at least

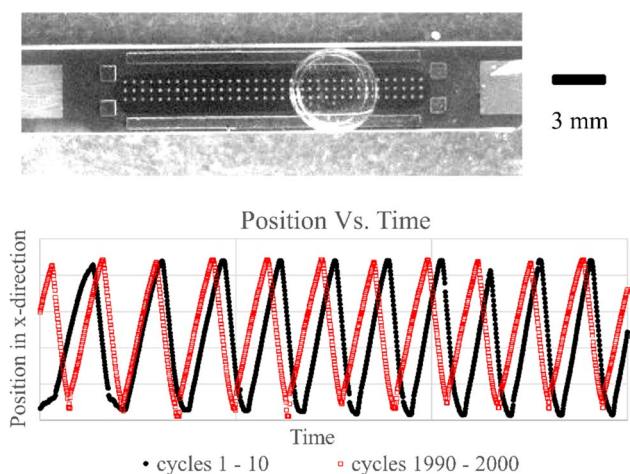


Fig. 9 Cyclic droplet actuation. *Top*: substrate used during testing. *Bottom*: the relative position versus time plot for the first and the final 10 cycles of the 2000 trials

two diode sites at all times. The number of the diode sites (12 in total) was rather small to provide conclusive evidence on the reliability of the diodes. In order to test the reliability of the proposed device, additional actuation substrates were fabricated with smaller device area and additional diodes. The device area was decreased to 18×3 mm, with the diodes being $100 \mu\text{m}$ in diameter and center to center spacing being $450 \mu\text{m}$ in three rows (Fig. 9, top).

All other parameters (including droplet volume ($60 \mu\text{L}$) and ambient fluid) were unchanged. The lower diode spacing brings more diodes into contact with the droplet and keeps the droplet potential closer to the potential of the rear edge. As a result, actuation voltages of 120 V achieved a droplet velocity of $\sim 5 \text{ mm/s}$. An overhead camera was triggered at 10 Hz to capture the location of the droplet while the droplet was repeatedly actuated back and forth the length of the actuator. Each testing cycle requires the droplet to travel from one end of the electrode to the other and back. Two thousand cycles were repeated for the reliability test. The position versus time of the initial 10 cycles and the final 10 cycles is plotted in Fig. 9, bottom. No degradation of the droplet actuation was observed visibly or in the velocity data. This is a substantial improvement over electrochemical diodes which only achieved 0–10 successful actuations.

8 Conclusion

In this paper, metal–semiconductor (Schottky barrier) diodes were embedded into the electrowetting substrate by evaporating titanium metal film onto low concentration n-type silicon. The resulting Schottky barrier was used as

replacement for the electrochemical diodes in bidirectional continuous electrowetting. From current–voltage measurements, it was found that electrochemical diodes based on passivation/etching metals could limit the performance of the device. By additional gold overlayer, the Schottky diodes were shielded from electrochemical reaction and improved device reliability. These devices achieved high actuation speeds of over 200 mm/s . After 2000 cycles of actuation, no device degradation was observed.

Unlike conventional electrowetting on dielectric actuation, bidirectional continuous electrowetting simplifies the control and fabrication needed for manipulating discrete droplets. This work demonstrated a reliable material system for continuous actuation. If this actuator was paired with position feedback, it could enable servo-style actuation. This would complement the dominant stepping actuation mode used in electrowetting and open additional possibilities to use droplet for mechanical actuation. The wiring simplification would be particularly powerful if implemented in a two-dimensional actuator.

Acknowledgments This work is supported in part by the National Science Foundation Grant No. CMMI-1130755. The authors would also like to acknowledge the support from the Research Experience for Undergraduates (REU) Program at the University of South Florida.

References

- Arscott S (2011) Moving liquids with light: photoelectrowetting on semiconductors. *Sci Rep* 1:184. doi:[10.1038/srep00184](https://doi.org/10.1038/srep00184)
- Arscott S (2014) Electrowetting and semiconductors. *RSC Adv* 4(55):29223–29238. doi:[10.1039/c4ra04187a](https://doi.org/10.1039/c4ra04187a)
- Bavière R, Boutet J, Fouillet Y (2007) Dynamics of droplet transport induced by electrowetting actuation. *Microfluid Nanofluid* 4(4):287–294. doi:[10.1007/s10404-007-0173-4](https://doi.org/10.1007/s10404-007-0173-4)
- Berge B (2005, 30 Jan.–3 Feb. 2005) Liquid lens technology: principle of electrowetting based lenses and applications to imaging. Paper presented at the micro electro mechanical systems, 2005. MEMS 2005. 18th IEEE international conference on
- Cho SK, Moon H, Kim C-J (2003) Creating, transporting, cutting, and merging liquid droplets by electrowetting-based actuation for digital microfluidic circuits. *J Microelectromech Syst* 12:70–80. doi:[10.1109/JMEMS.2002.807467](https://doi.org/10.1109/JMEMS.2002.807467)
- Crane NB, Volinsky AA, Mishra P, Rajgadkar A, Khodayari M (2010) Bidirectional electrowetting actuation with voltage polarity dependence. *Appl Phys Lett* 96(10):104103. doi:[10.1063/1.3353990](https://doi.org/10.1063/1.3353990)
- Dhindsa M, Heikenfeld J, Weekamp W, Kuiper S (2011) Electrowetting without electrolysis on self-healing dielectrics. *Langmuir* 27(9):5665–5670
- Gong J, Kim CJ (2008) All-electronic droplet generation on-chip with real-time feedback control for EWOD digital microfluidics. *Lab Chip* 8(6):898–906. doi:[10.1039/b717417a](https://doi.org/10.1039/b717417a)
- Hayes RA, Feenstra BJ (2003) Video-speed electronic paper based on electrowetting. *Nature* 425(6956):383–385
- Jaeger RC (2002) Introduction to microelectronic fabrication, 2nd edn. Prentice Hall, Upper Saddle River

- Khodayari M, Carballo J, Crane NB (2012a) A material system for reliable low voltage anodic electrowetting. *Mater Lett* 69:96–99. doi:[10.1016/j.matlet.2011.11.060](https://doi.org/10.1016/j.matlet.2011.11.060)
- Khodayari M, Carballo J, Crane NB (2012b) A material system for reliable low voltage anodic electrowetting. *Mater Lett* 69(3):96–99. doi:[10.1016/j.matlet.2011.11.060](https://doi.org/10.1016/j.matlet.2011.11.060)
- Khodayari M, Hahne B, Crane NB (2014) Long life electrochemical diodes for continuous electrowetting. *J Electrochem Soc* 161(6):E105–E111. doi:[10.1149/2.008406jes](https://doi.org/10.1149/2.008406jes)
- Knospe CR, Haj-Hariri H (2012) Capillary force actuators: modeling, dynamics, and equilibria. *Mechatronics* 22(3):251–256. doi:[10.1016/j.mechatronics.2011.07.007](https://doi.org/10.1016/j.mechatronics.2011.07.007)
- Lee J, Kim CJ (2000) Surface-tension-driven microactuation based on continuous electrowetting. *J Microelectromech Syst* 9(2):171–180. doi:[10.1109/84.846697](https://doi.org/10.1109/84.846697)
- Moon I, Kim J (2006) Using EWOD (electrowetting-on-dielectric) actuation in a micro conveyor system. *Sens Actuators Phys* 130:537–544. doi:[10.1016/j.sna.2005.12.016](https://doi.org/10.1016/j.sna.2005.12.016)
- Mugele F, Baret J-C (2005) Electrowetting: from basics to applications. *J Phys: Condens Matter* 17:R705–R774. doi:[10.1088/0953-8984/17/28/R01](https://doi.org/10.1088/0953-8984/17/28/R01)
- Nelson WC, Kim CJ (2012) Droplet actuation by electrowetting-on-dielectric (EWOD): a review. *J Adhes Sci Technol* 26(12–17):1747–1771. doi:[10.1163/156856111x599562](https://doi.org/10.1163/156856111x599562)
- Nelson CW, Lynch CM, Crane NB (2011) Continuous electrowetting via electrochemical diodes. *Lab Chip* 11(13):2149–2152. doi:[10.1039/c1lc20196d](https://doi.org/10.1039/c1lc20196d)
- Nguyen N-T, Ng KM, Huang X (2006) Manipulation of ferrofluid droplets using planar coils. *Appl Phys Lett* 89(5):052509. doi:[10.1063/1.2335403](https://doi.org/10.1063/1.2335403)
- Ni Q, Capecci DE, Crane NB (2015) Electrowetting force and velocity dependence on fluid surface energy. *Microfluid Nanofluid* 19(1):181–189. doi:[10.1007/s10404-015-1563-7](https://doi.org/10.1007/s10404-015-1563-7)
- Ni Q, Capecci DE, Crane NB (2016) Open-loop electrowetting actuation with micro-stepping. *Sens Actuators A* 247:579–586. doi:[10.1016/j.sni.2016.06.034](https://doi.org/10.1016/j.sni.2016.06.034)
- Olikh OY (2015) Review and test of methods for determination of the Schottky diode parameters. *J Appl Phys* 118(2):024502. doi:[10.1063/1.4926420](https://doi.org/10.1063/1.4926420)
- Pollack MG, Fair RB, Shenderov AD (2000) Electrowetting-based actuation of liquid droplets for microfluidic applications. *Appl Phys Lett* 77(11):1725–1726. doi:[10.1063/1.1308534](https://doi.org/10.1063/1.1308534)
- Ren H, Fair RB, Pollack MG, Shaughnessy EJ (2002) Dynamics of electro-wetting droplet transport. *Sens Actuators B: Chem* 87(1):201–206. doi:[10.1016/s0925-4005\(02\)00223-x](https://doi.org/10.1016/s0925-4005(02)00223-x)
- Sen P, Kim CJ (2009) A fast liquid-metal droplet microswitch using EWOD-driven contact-line sliding. *J Microelectromech Syst* 18(1):174–185. doi:[10.1109/Jmems.2008.2008624](https://doi.org/10.1109/Jmems.2008.2008624)
- Takei A, Matsumoto K, Shomoyama I (2010) Capillary motor driven by electrowetting. *Lab Chip* 10:1781–1786. doi:[10.1039/c001211d](https://doi.org/10.1039/c001211d)
- Wixforth A, Strobl C, Gauer C, Toegl A, Scriba J, v Guttenberg Z (2004) Acoustic manipulation of small droplets. *Anal Bioanal Chem* 379(7–8):982–991. doi:[10.1007/s00216-004-2693-z](https://doi.org/10.1007/s00216-004-2693-z)